Variation of elastic scattering across a quantum well

G. Salis, P. Wirth, T. Heinzel, T. Ihn, and K. Ensslin
Solid State Physics Laboratory, ETH Zürich, 8093 Zürich, Switzerland

K. Maranowski and A. C. Gossard
Materials Department, University of California, Santa Barbara, Ca 93106, USA
(November 28, 2017)

The Drude scattering times of electrons in two subbands of a parabolic quantum well have been studied at constant electron sheet density and different positions of the electron distribution along the growth direction. The scattering times obtained by magnetotransport measurements decrease as the electrons are displaced towards the well edges, although the lowest-subband density increases. By comparing the measurements with calculations of the scattering times of a two-subband system, new information on the location of the relevant scatterers and the anisotropy of intersubband scattering is obtained. It is found that the scattering time of electrons in the lower subband depends sensitively on the position of the scatterers, which also explains the measured dependence of the scattering on the carrier density. The measurements indicate segregation of scatterers from the substrate side towards the quantum well during growth.

The striking success of Ga[Al]As semiconductor heterostructures originates from the extremely high mobilities obtained in these materials. One key ingredient for the fabrication of such samples is modulation doping, where dopants and electrons are spatially separated. At low temperatures, impurity scattering, alloy scattering and interface roughness scattering limit the electron mobility [1]. If more than one subband is occupied, intersubband scattering takes place in addition [2,3].

Information on the relevant scattering processes is usually obtained by measuring how quantum ($\tau_{\rm q}$) and Drude scattering times (τ) vary with carrier density $n_{\rm S}$. For two-dimensional electron gases (2DEGs) realized in AlGaAs heterostructures, it is found that impurity scattering is dominant. In this case, one finds $\tau \propto n_{\rm S}^{\gamma}$, with γ between 1 and 1.5, depending on the distance between the dopants and the 2DEG [1].

In a two-subband system with subband densities n_1 and n_2, the Drude scattering times τ_i of subband i are usually found to increase monotonically with n_i [4,5]. Recent results show that in a parabolic quantum well (PQW), τ_1 may also slowly decrease, i.e. $\gamma < 0$, when a second subband is occupied [6]. In this paper, we investigate this unusual dependence and show that it may be due to a certain arrangement of the ionized impurities.

The PQW, grown by molecular beam epitaxy (MBE), is a 760 Å wide $Al_xGa_{1-x}As$ layer with x varying parabolically between 0 and 0.1 [7] (inset of Fig. 1a). In the center of the well, a three monolayer thick $Al_{0.05}Ga_{0.95}As$ layer forms a potential spike. The well is embedded symmetrically in 200 Å of undoped $Al_{0.3}Ga_{0.7}As$ spacer layers and remote Si-doping layers on both sides. On the surface side, the donors are provided by 11 sheets, each with a Si donor density of nominally $5{\cdot}10^{15}\,\mathrm{m}^{-2}$

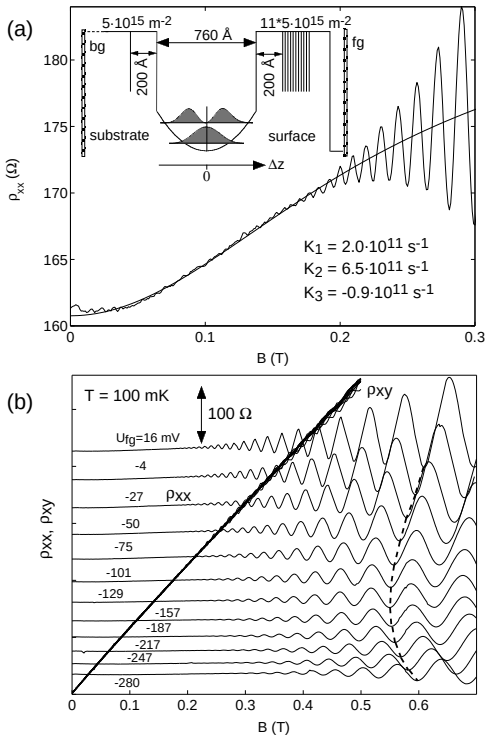

FIG. 1. (a) Fit of $\rho_{xx}(B)$ for V_{fg}=-50 mV ($V_{\rm bg}$=+1000 mV) to the two-subband scattering model. Inset: scheme of sample layout along the growth direction. (b) Measured ρ_{xx} for different electron positions along the growth direction at $n_{\rm S} = 2.9 \cdot 10^{15}\,\mathrm{m}^{-2}$. Values for $U_{\rm fg}$ are indicated, and $U_{\rm bg}$ is varied between -2.2 V (top) and +2.2 V (bottom) in steps of 0.4 V. Subsequent data are offset for clarity by 50 Ω. From top to bottom, the electron distribution is displaced towards the substrate. The data for ρ_{xy} fall on top of each other since $n_{\rm S}$ is constant. Minima corresponding to the same filling factor in the lower subband are connected by a dashed line.

Si-concentration, arranged in a 200 Å thick layer. On the substrate side, the donors are located within one δ-doping layer with a concentration of $5{\cdot}10^{15}\,\mathrm{m}^{-2}$. This asymmetry in the doping allows for saturation of the surface states and an effectively symmetric location of the electron distribution in the well. A back gate electrode consists of a 250 Å thick n^+-doped layer located 1.35 μm below the well. A TiPtAu front gate electrode was evaporated on top of the structure. The experiments were carried out with standard Hall-bar geometries at temperatures of 100 mK. A magnetic field B was applied perpendicular to the electron gas.

Figure 1a shows a measurement of the magnetoresistivity $\rho_{xx}(B)$ at $n_\mathrm{S} = 2.9 \cdot 10^{15}\,\mathrm{m}^{-2}$. From the low-field magnetoresistivity, τ_1 and τ_2 are obtained. Early studies on scattering times in two-subband systems relied on the assumption of two independent electronic systems with additive conductivities $\sigma = \sigma_1 + \sigma_2$ with $\sigma_i = n_i e^2 \tau_i / m$, quantitatively explaining a measured positive magnetoresistance [4,8,9] (e,m electron charge and effective mass). In a more sophisticated model based on the Boltzmann equation [5], intersubband scattering is taken explicitly into account. This leads to B-dependent scattering times

$$\tau_i(B) = \mathrm{Re}\left(\sum_j (\mathbf{K} + i\omega_c \mathbf{1})^{-1}_{ij} k_j / k_i \right), \qquad (1)$$

where the k_i are the Fermi wave vectors, $k_i = \sqrt{2\pi n_i}$, $\omega_c = eB/m$, and $\mathbf{K}$ the scattering matrix defined by

$$\begin{pmatrix} K1 & K3 \\ K3 & K2 \end{pmatrix} = \begin{pmatrix} P_{00}^{(0)} - P_{00}^{(1)} + P_{10}^{(0)} & -P_{10}^{(1)} \\ -P_{10}^{(1)} & P_{11}^{(0)} - P_{11}^{(1)} + P_{10}^{(0)} \end{pmatrix} \qquad (2)$$

The coefficients $P_{nm}^{(i)}$ are related to the transition rates $P_{nm}(\phi)$ between subband states n and m and scattering angle ϕ by Fourier transformation in ϕ. $P_{ij}^{(0)}$ is the transition rate integrated over the allowed scattering vectors, while in $P_{ij}^{(1)}$ the integrand is multiplied by $\cos\phi$. The difference $P_{ii}^{(0)} - P_{ii}^{(1)}$ corresponds to the single-subband Drude scattering rate, where the matrix element of the scattering potential is weighted by $(1 - \cos\theta)$. Note that in the diagonal elements, also the isotropic part of intersubband scattering is included. We have shown in a recent paper that intersubband scattering cannot be neglected in our experiments [6].

With n_i known, Eq. 1 allows a fit to $\rho_{xx}(B)$, with K_1, K_2 and K_3 being the fit parameters [5,6] (Fig. 1a).

We measured $\rho_{xx}(B)$ at $n_\mathrm{S} = 2.9 \cdot 10^{15}\,\mathrm{m}^{-2}$ (controlled by the low-field Hall voltage) and different positions of the electron distribution along the growth direction (Fig. 1b). The electrons were displaced by applying voltages U_fg (U_bg) between the front (back) gate electrode and the electron gas.

Clearly visible are variations of both amplitude and period of the Shubnikov-de Haas (SdH) oscillations with changing V_fg. The amplitudes at a fixed magnetic field decay as the wave functions are displaced towards the substrate. This corresponds to a decreasing τ_q [3,10], an effect not to be discussed in this paper (see Ref. [6] for evaluated data on τ_q).

By fitting U_bg as a function of U_fg at constant n_S to a capacitor model, we find the displacement Δz per front gate voltage to be about 1000 Å/V [11]. Thus we can plot the data as a function of Δz instead of gate voltages. From the SdH frequency we evaluate $n_1(\Delta z)$ (Fig. 2a). A minimum occurs in n_1 at $U_\mathrm{fg} \approx -130\,\mathrm{mV}$ and is related to the narrow potential spike in the center of the PQW. The spike leads to subband energy shifts depending sensitively on the electron distribution along the growth direction. A displacement of the electrons thus changes n_1 and n_2. The difference between the two lowest subband energies reaches a minimum when the wave functions are centered with respect to the spike. Therefore, the minimum in n_1 provides the reference for the location of the wave functions in growth direction [12], where $\Delta z = 0$.

From the data, we evaluated τ_1 and τ_2 for different Δz (Fig. 2a). Both τ_1 and τ_2 show a maximum as a function of Δz. The maximum in τ_2 occurs where wave functions are centered, i. e. $\Delta z = 0$.

Assuming a decrease of τ_i with decreasing n_i ($\gamma > 0$), we expect a minimum in τ_1 at $\Delta z = 0$, which disagrees with the measurement. On the other hand, the scattering rate depends on the distances from the relevant scatterers [13]. For $\Delta z = 0$, these distances are maximized, giving rise to large τ_i. The fact that τ_1 is large around $\Delta z = 0$ indicates that not its density-dependence dominates τ_1, but the distance to the relevant scatterers. In contrast to the first subband, both, n_2 and τ_2 have a maximum at $\Delta z = 0$. Note that n_2 is much smaller than n_1, leading to small Fermi wave numbers where screening is more efficient. Thus the screened scattering potential at relevant wave numbers is less sensitive to displacements along the growth direction. On the other hand, the relative change of n_2 with Δz is larger than that of n_1. Hence, τ_2 is stronger influenced by its density dependence than by Δz, which explains the coincidence of the maximum in τ_2 with $\Delta z = 0$.

The maximum of τ_1 is shifted towards the surface, indicating stronger scattering on the substrate side. Although this could be explained by assuming more dopants than expected from the MBE growth protocol, we can excluded this, because the total amount of Si brought on the wafer was measured accurately. However there might be segregation of dopants on the substrate side towards the PQW during growth, which enhances scattering significantly. As we will show, a calculation of the τ_i supports the assumption of segregated Si atoms.

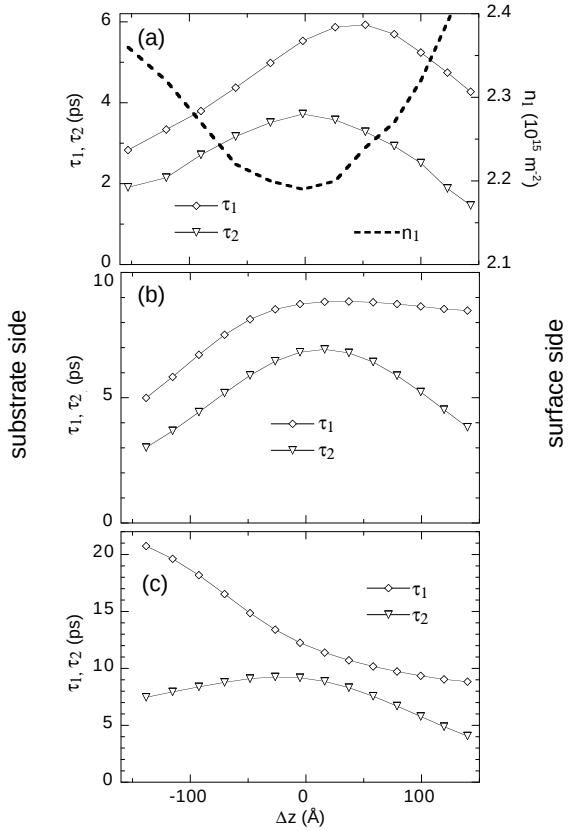

FIG. 2. (a) Measurement of τ_1, τ_2 and n_1 vs Δz at $n_S = 2.9 \cdot 10^{15}\,\mathrm{m}^{-2}$. (b) Calculated scattering times with $1.5 \cdot 10^{15}\mathrm{m}^{-2}$ of dopants shifted towards the substrate-sided edge of the parabolic profile. (c) The same calculations as in (b), but with a distribution of scatterers as in the growth protocol.

The matrix elements of the scattering potential were obtained by numerical integration using self-consistently calculated wave functions [14]. Then the transition rates $P_{nm}^{(i)}$ were calculated by integrating the squared matrix elements over the allowed scattering vectors. Screening was included in the Thomas Fermi approximation. The τ_i were calculated from Eq. 1. A detailed calculation of the scattering rates based on different scattering mechanisms reveals that the contributions of alloy scattering (including the potential spike) and interface roughness scattering are an order of magnitude smaller than that of Coulomb scattering. Initially, two layers of Coulomb scatteres were included. The dopants on the surface side were gathered in a single δ-layer 300 Å above the well, with a concentration of $N_1 = 3 \cdot 10^{16}\,\mathrm{m}^{-2}$. The second layer is the doping layer 200 Å below the well ($N_2 = 2.8 \cdot 10^{15}\,\mathrm{m}^{-2}$). These values correspond to half of the nominal Si concentration brought on the wafer during the MBE-growth, qualitatively accounting for deep donors and not ionized impurities. Figure 2b shows the obtained scattering times. As expected for this donor configuration, τ_1 monotonically increases as the electrons are displaced towards the substrate side.

In order to take segregated Si atoms into account, we placed $N_3 = 1.5 \cdot 10^{15}\,\mathrm{m}^{-2}$ scatterers at the edge of the well on the substrate side, and reduced N_2 by the same amount (Fig 2c). As in the experiment, we obtain a maximum in τ_1 displaced towards the surface side and a maximum of τ_2 at $\Delta z = 0$. At the surface side, τ_1 decreases only slowly, saturating at a value comparable to the simulation with $N_3 = 0$. It is the balance between the monotonically decrasing τ_1 shown in Fig. 2c, and the range and strength of the extra layer, which determines the exact shape of $\tau_1(\Delta z)$

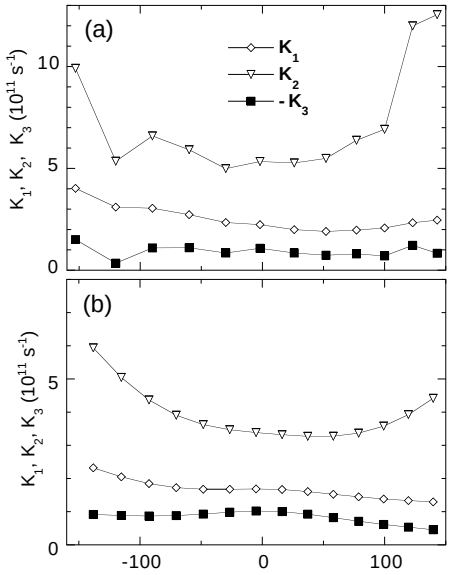

FIG. 3. Measured (a) and calculated (b) K_1, K_2 and $-K_3$. In (b), ionized impurity scattering was modelled as in Fig.2c.

The calculated scattering times are about 50 percent larger than the measured ones. It is well-known that for PQWs calculations overestimate the scattering times. Possible explanations are size-effect scattering from the edges of the electron gas [15] or enhanced background impurities due to the greater reactivity of Al with oxygen and carbon-containing molecules in the MBE chamber. In addition, the calculated values depend on how screening of the scattering potential is implemented and which concentration of ionized impurities is assumed. We did not attempt to simulate τ_i accurately, here only the qualitative behavior, in particular its spatial dependence, is of importance.

Additional insight can be gained by studying the spatial variation of the matrix elements K_i (Fig. 3a). Usually, Drude times are insensitive to small-angle scattering. For intersubband scattering, K_3 contains the part of the scattering rate weighted by $\cos\phi$. This gives information about the amount of small-angle intersubband scattering. Since almost no structure in K_3 is observed,

while K_1 increases stronger on the substrate side, large-angle scattering must be higher on the substrate side. In order to increase large-angle scattering of Coulomb scatterers with fixed density, the distance to the electron gas has to be diminished. This happens if scatterers segregate towards the electron gas. The calculated K_i nicely reproduce the experimental data (Fig 3b).

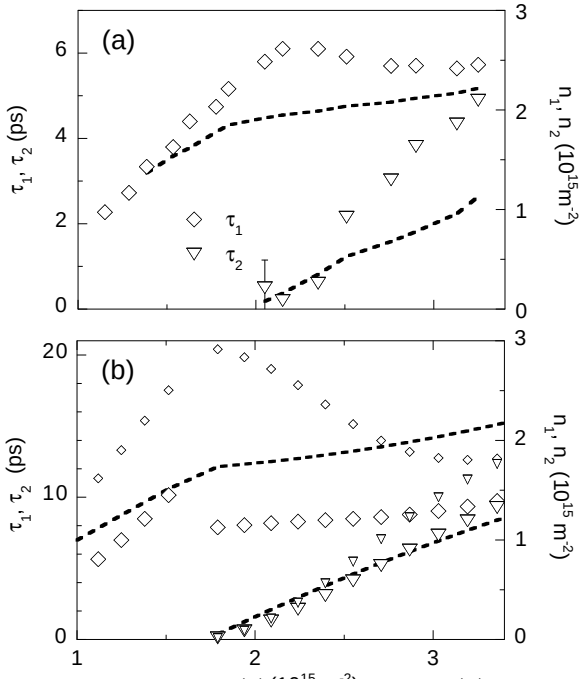

FIG. 4. Measurements (a) and calculation (b) of scattering times (symbols) and subband densities (lines) vs n_S. In (b), small symbols are calculated without, large symbols with additional impurities at the substrate side of the well.

With this strong evidence for segregated scatterers at the substrate side of the well, we come back to the previously unexplained structure in the density-dependence of τ_i [6]. In this experiment, $U_{\rm bg}$ was kept fixed, while $U_{\rm fg}$ and therefore n_s was changed. In Fig. 4, the measured and calculated values for τ_1, τ_2, n_1 and n_2 are shown. In the measurement, τ_1 slightly decreases as n_2 gets populated. In the calculation, the additional scattering layer gives rise to a weak increase of τ_1 with $n_{\rm S}$ when the second subband is occupied (large symbols), whereas a steep decrease results in the case of no additional layer (small symbols). Thus the additional scatters are responsible for the slope of $\tau_1(n_{\rm S})$. Since $n_{\rm S}$ is driven by $V_{\rm fg}$, the electron distribution expands towards the surface side with increasing $n_{\rm S}$. Thus the scatterers on both sides of the well compete and determine the shape of $\tau(n_{\rm S})$. As discussed above, for small n_2, τ_2 is not so much sensitive to additional scatterers, which is reflected in similar values obtained from the two simulations shown in Fig. 4b.

In conclusion, we have presented an investigation of Drude scattering times in a modulation-doped multi-subband quantum well. Using front- and back gate voltages, the position of the electron distribution and the subband densities were tuned. The Drude scattering times of individual subbands were measured. It was found that τ_1 is dominated by the distance of the 2DEG to the impurities and not by its density dependence. Its behavior could therefore be used to locate additional scatterers at the substrate edge of the well, which are presumably due to segregation of dopants during growth. The measured scattering times could be qualitatively reproduced in a calculation assuming that half of the substrate-sided donors had diffused to the edge of the well. Using these results, previous measurements of the density dependence of τ_1 could be explained. While obtained for a PQW, the presented method of investigating the scattering times as a function of the electron-gas position might give further informations on scatterererers in other types of samples.

We acknowledge valuable discussions with J. Blatter, P. Coleridge, K. v. Klitzing, P. Petroff and E. Zaremba. This project was financially supported by the Swiss Science Foundation and AFOSR grant F 49620-94-1-0158.

[1] T. Ando, J. Phys. Soc. of Jpn. **51**, 3900 (1982); A. Gold, Phys. Rev. B **38**, 10798 (1988).
[2] E. D. Siggia and P. C. Kwok, Phys. Rev. B **2**, 1024 (1970); S. Mori and T. Ando, Phys. Rev. B **19**, 6433 (1979), H. L. Störmer, A. C. Gossard, and W. Wiegmann, Solid State Comm. **41**, 707 (1982).
[3] T. Ando, A. B. Fowler, and F. Stern, Rev. Mod. Phys. **54**, 437 (1982).
[4] T. P. Smith III, and F. F. Fang, Phys. Rev. B **37**, 4303 (1988).
[5] E. Zaremba, Phys. Rev. B **45**, 14143 (1992).
[6] T. Heinzel, G. Salis, K. Ensslin, K. Maranowski, and A. C. Gossard, Physica B, in print.
[7] A. C. Gossard, IEEE J. Quant. Electron. **22**, 1649 (1986).
[8] H. van Houten, J. G. Williamson, M. E. I. Broekaart, C. T. Foxon, and J. J. Harris, Phys. Rev. B **37**, 2756 (1988).
[9] T. P. Smith III, F. F. Fang, U. Meirav, and M. Heiblum, Phys. Rev. B **38**, 12744 (1988).
[10] P. T. Coleridge, R. Stoner, and R. Fletcher, Phys. Rev. B **39**, 1120 (1989).
[11] G. Salis, K. Ensslin, K. B. Campman, K. Maranowski, and A. C. Gossard, Physica B **251**, 941 (1998).
[12] G. Salis, B. Graf, K. Ensslin, K. Campman, K. Maranowski, and A. C. Gossard, Phys. Rev. Lett. **79**, 5106 (1997).
[13] M. Heiblum, E. E. Mendez, and F. Stern, Appl. Phys. Lett. **44**, 1064 (1984).
[14] We used a one-dimensional Poisson-Schrödinger solver written by G. Snider.
[15] W. Walukiewicz, P. F. Hopkins, M. Sundaram, and A. C. Gossard, Phys. Rev. B **44**, 10909, 1991.